Electronic Supplementary Material (ESI) for Journal of Materials Chemistry A.

Supporting information

Increase and Discretization of the Energy Barrier for Individual $LiNi_xCo_yMn_zO_2$ (x+2y =1) Particles with the Growth of a Li_2CO_3 Surface Film

Kun Qian [1, 3], Binhua Huang [2, 3], Yuxiu Liu [2, 3], Marnix Wagemaker [4], Ming Liu [4], Huan Duan [2], Dongqing Liu2, Yan-Bing He [2], Baohua Li [2], & Feiyu Kang[1, 2, 3]

[1] Shenzhen Environmental Science and New Energy Technology Engineering Laboratory, Tsinghua-Berkeley Shenzhen Institute, Shenzhen 518055, P. R. China.

[2] Engineering Laboratory for the Next Generation Power and Energy Storage Batteries, Graduate School at Shenzhen, Tsinghua University, Shenzhen 518055, China.

[3] Laboratory of Advanced Materials, School of Materials Science and Engineering, Tsinghua University, Beijing 100084, PR China.

[4] Department of Radiation Science and Technology, Faculty of Applied Sciences, Delft University of Technology, Mekelweg 15, 2629 JB, Delft, The Netherlands

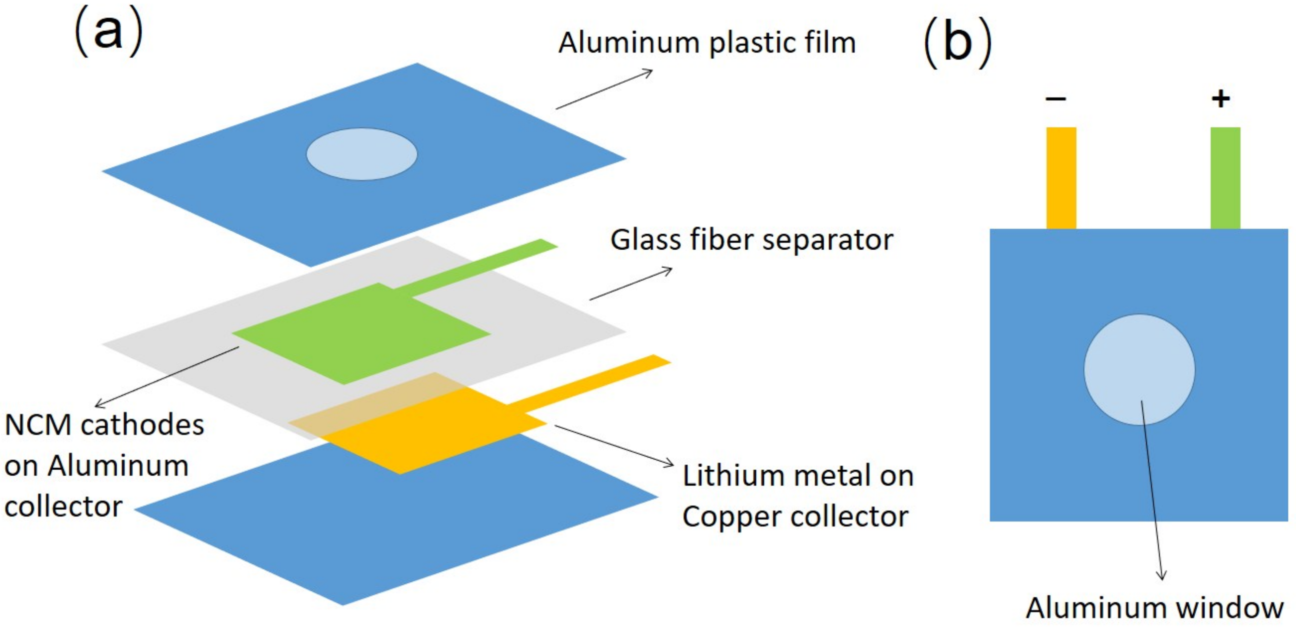

Figure S1 Schematics of *in-situ* X-ray diffraction battery. (a) The inner structure of the *in-situ* pouch cell. It is consisted of a working electrode, a metallic lithium as counter electrode, electrolyte and glass fiber separator. Those components are sealed with Aluminum plastic film. (b) A Aluminum window on cathodes side is specially designed for the X-ray penetration and detection on the crystal change of NCM materials during cycling. The *in-situ* cells were assembled in a Mbraun glove box ($O_2 < 0.1$ ppm, $H_2O < 0.1$ ppm) with a vacuum packaging machine (Audionvac VMS 153).

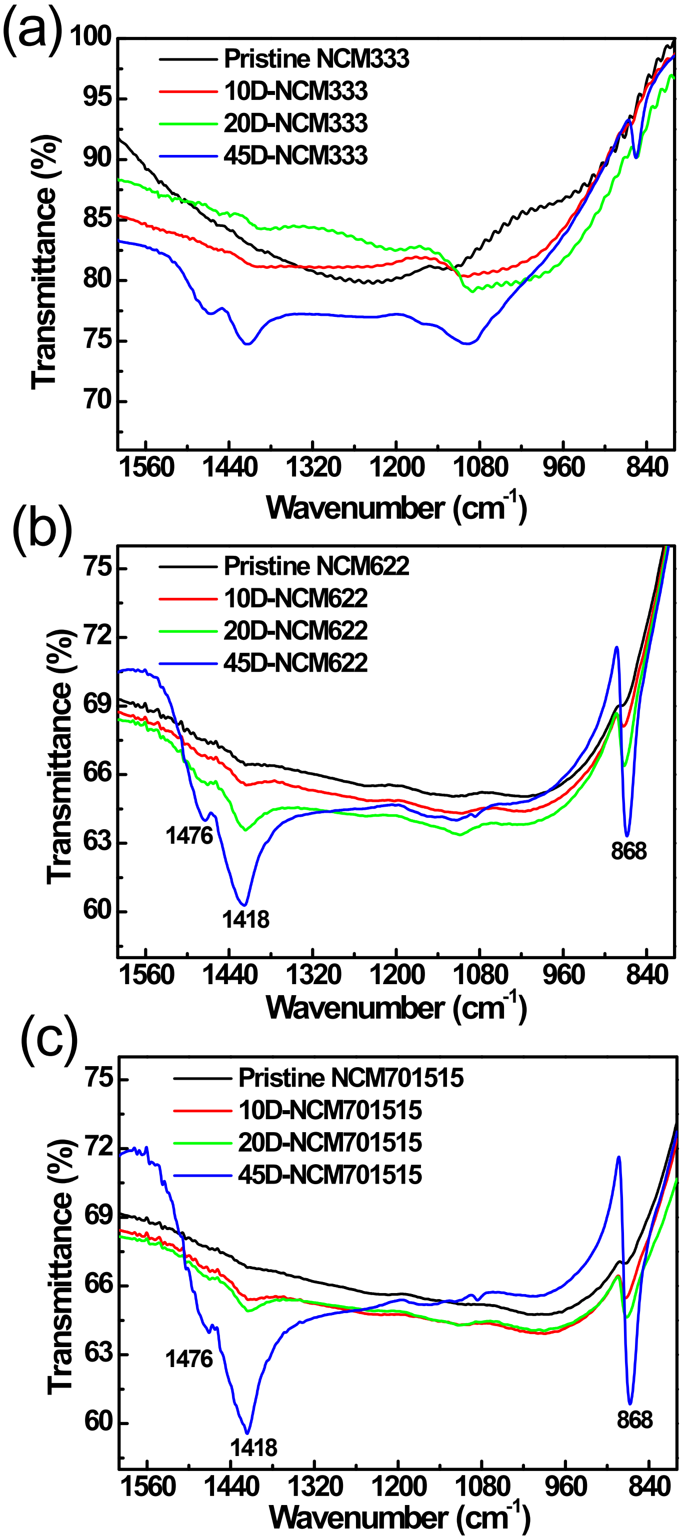

Figure S2 FT-IR ATR spectra of (a) NCM333, (b) NCM622 and (c) NCM701515. It can be seen that the characteristic peaks of Li_2CO_3 at 1476 cm^{-1}, 1418^{-1} and 868 cm^{-1} increase with the storage time prolongs, which indicate the growth of Li_2CO_3 film. With the increase of Ni-content, the evolution of Li_2CO_3 peaks become more and more obvious.

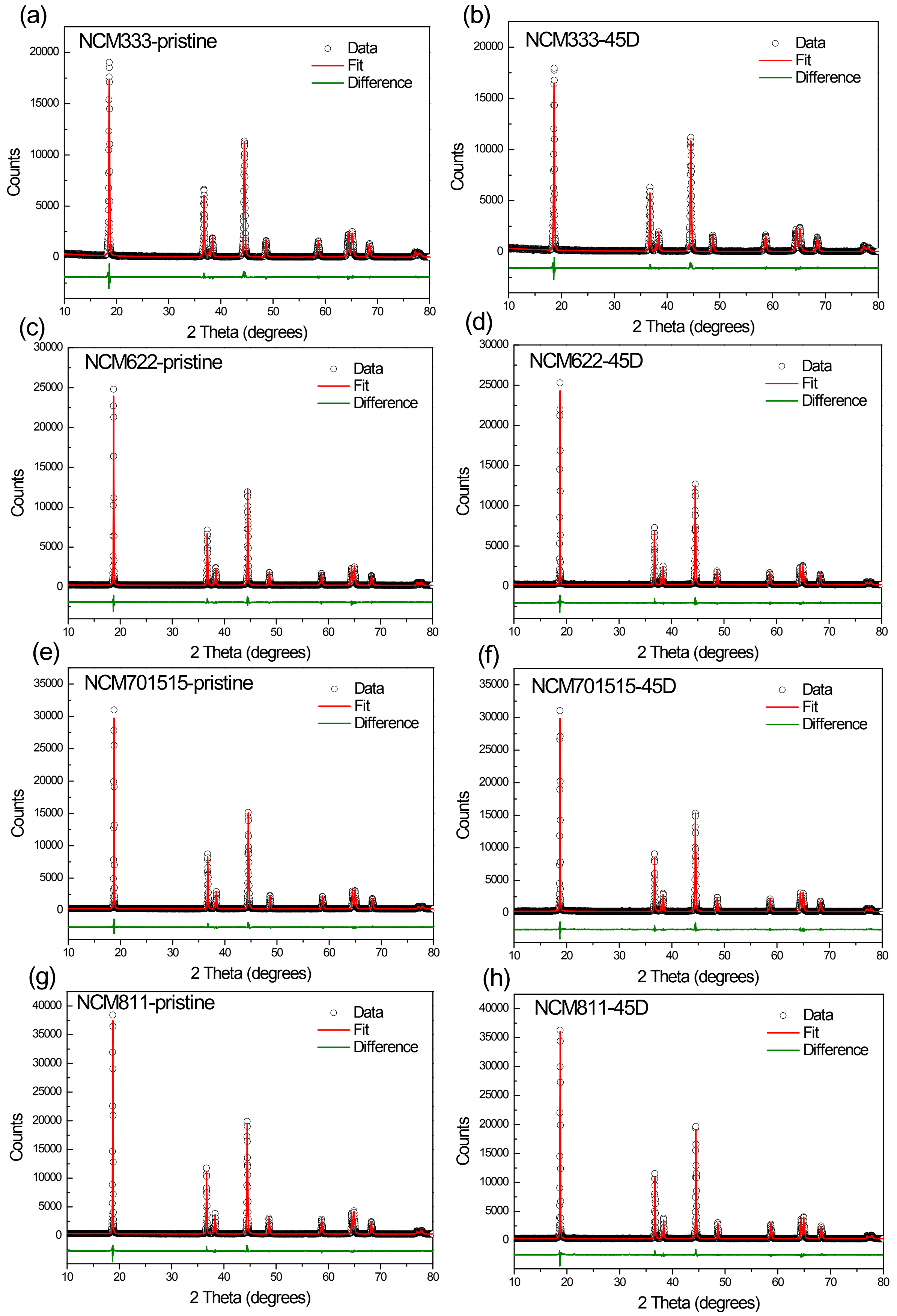

Figure S3 Rietveld refinements of XRD patterns for NCM samples were performed before and after 45 days' storage. The figures shows single-phase fitting of the layered oxides with space group of $R\bar{3}m$. The detailed cell parameters for each sample were summarized in Table S2. Refinements of the crystal structure confirm that the bulk of NCMs did not change during storage. The damage mainly come from the degradation of crystal surface.

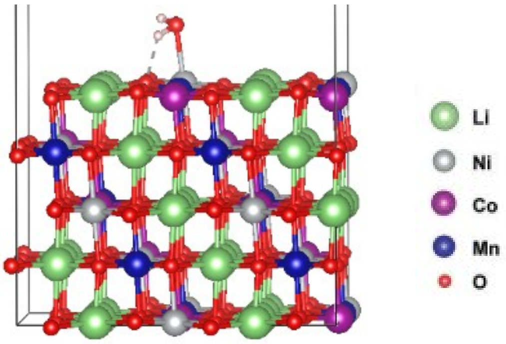

NCM333

Figure S4 Density functional theory (DFT) calculations of water molecule adsorption on the NCM

Density functional theory (DFT) calculations were performed with the all-electron code Fritz-Haber Institute *ab initio* molecules simulations package (FHI-aims)[1]. The exchange-correlation potentials were treated by the generalized gradient approximation (GGA) parametrized by Perdew, Burke, and Ernzerholf (PBE)[2]. The DFT+U method[3] was adopted to offer an ad hoc correction for strongly correlated systems which includes the 3d orbitals of Ni, Co and Mn ions at negligible computation cost. Spin-polarized magnetic configurations were considered in all cases. Periodic nonpolar ($10\bar{1}4$) surface slabs were proposed to simulate the adsorption process, and the vacuum layer between neighboring models was at least 20 Å to reduce the electrostatic interactions between them. The Brillion zone was sampled by an appropriate Monkhorst-Pack grid with a density of at least 0.03 $Å^{-1}$.[4] The bottom two layers were fixed and the top three layers and all adsorbates were relaxed until the charge density and the total energy were below of 10^{-4} eV/$Å^3$ and 10^{-5} eV, respectively. To account for the vdW interactions between molecules and solid surfaces, the vdW^{surf} approach was employed with the Tkatchenko and Scheffler scheme.[5]

The DFT adsorption energy of the water molecule, which describes the stability of the system, were calculated by

$$\Delta E_{ads} = E_{system} - E_{substrate} - E_{water} \tag{1}$$

where E_{system} is the total energy for a water molecule adsorbed on the NCM substrate, $E_{substrate}$ is the total energy for the NCM cathode system without molecule adsorption, and $E_{water}$is the total energy of a separated water molecule as determined from DFT calculations.

Adsorption Site	**Ni**	**Co**	**Mn**
Adsorption Energy (eV)	-0.98	-0.37	-0.54

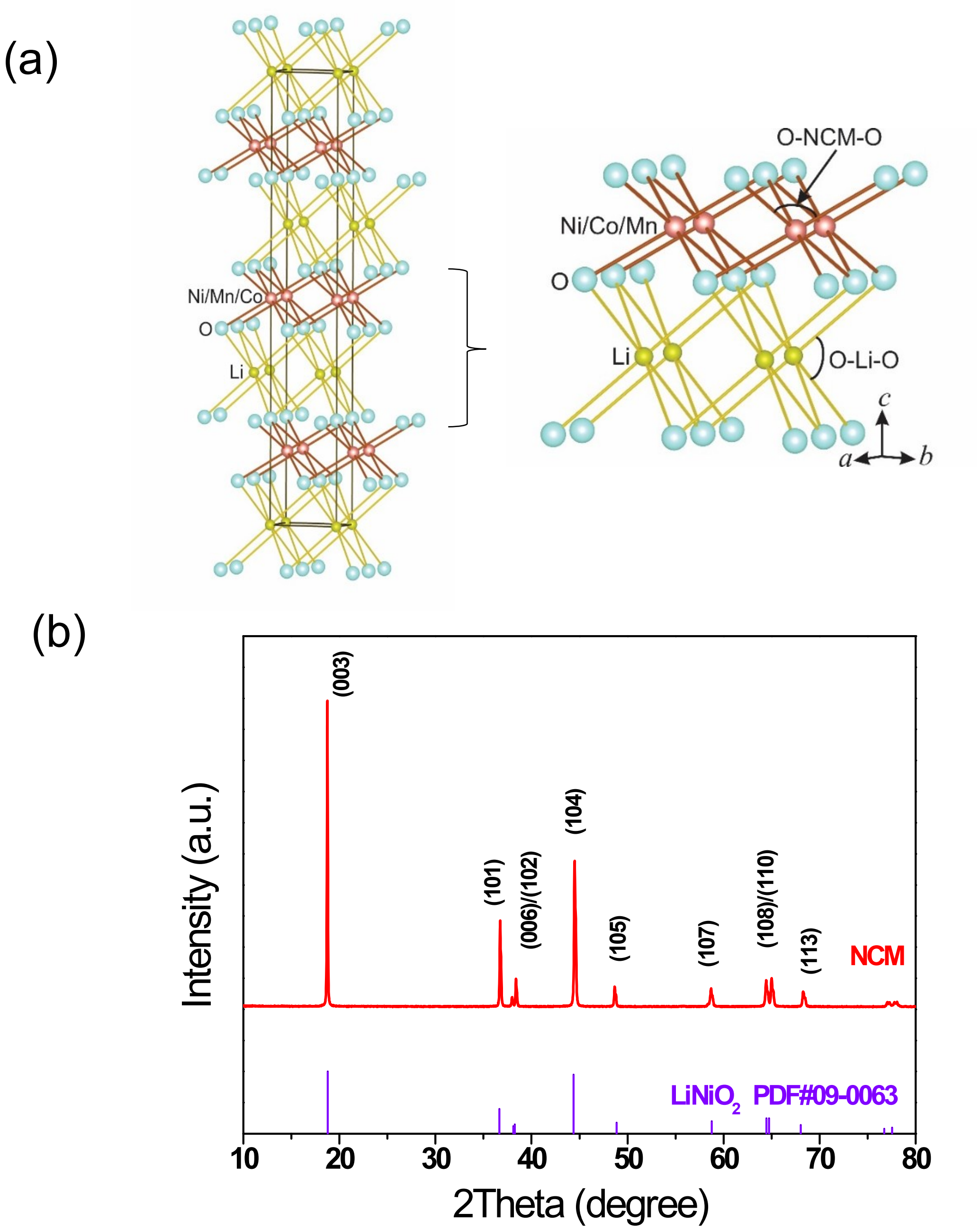

Figure S5 (a) Crystal structure of layered NCM cathodes. NCMs possess a typical α-$NaFeO_2$ type hexagonal structure with ($R\bar{3}m$) symmetry. This structure has Li-ions at the 3a, the transition metal ions (Ni, Co, Mn) at 3b and O ions at 6c sites. It also can be viewed as well-ordered stacked Li layer-transition metal oxides slab (Li-TM oxides) along c axis. Li ions are sandwiched between two TM oxides slabs. Based on the ratio of Ni, Co and Mn ions in the TM layer, different materials with similar crystal structures such as NCM333, NCM622 and NCM811 are defined in this paper. (b) Typical XRD pattern for NCM cathodes. The (003) peak is the strongest peak, which mainly reflects the crystal information along *c* axis. With the extension along the *c* axis, the (003) peak will shift to a small 2θ. While the contraction along the *c* axis would lead to the shift to a large 2θ [6] Since the similar ion radius of Li and Ni, a partial interchange of occupancy of Li and Ni is found in NCM cathodes, which is called 'cation mixing' and it is believed to have a negative impact on overall electrochemical performance. Besides, the oxygen sub lattice in the crystal structure is considered as distorted from the fcc array in the direction of hexagonal *c* axis. [7] This distortion gives rise to a splitting of the lines assigned to the Miller indices (006, 102) and (108, 110) in the XRD patterns and these are also characteristic of the layered structure. The Rietveld refinements in Figure S3 and Tables S2 provide the detailed cell parameter of NCM333, NCM622, NCM701515 and NCM811 including the *a*, *b*, *c* and cation mixing.

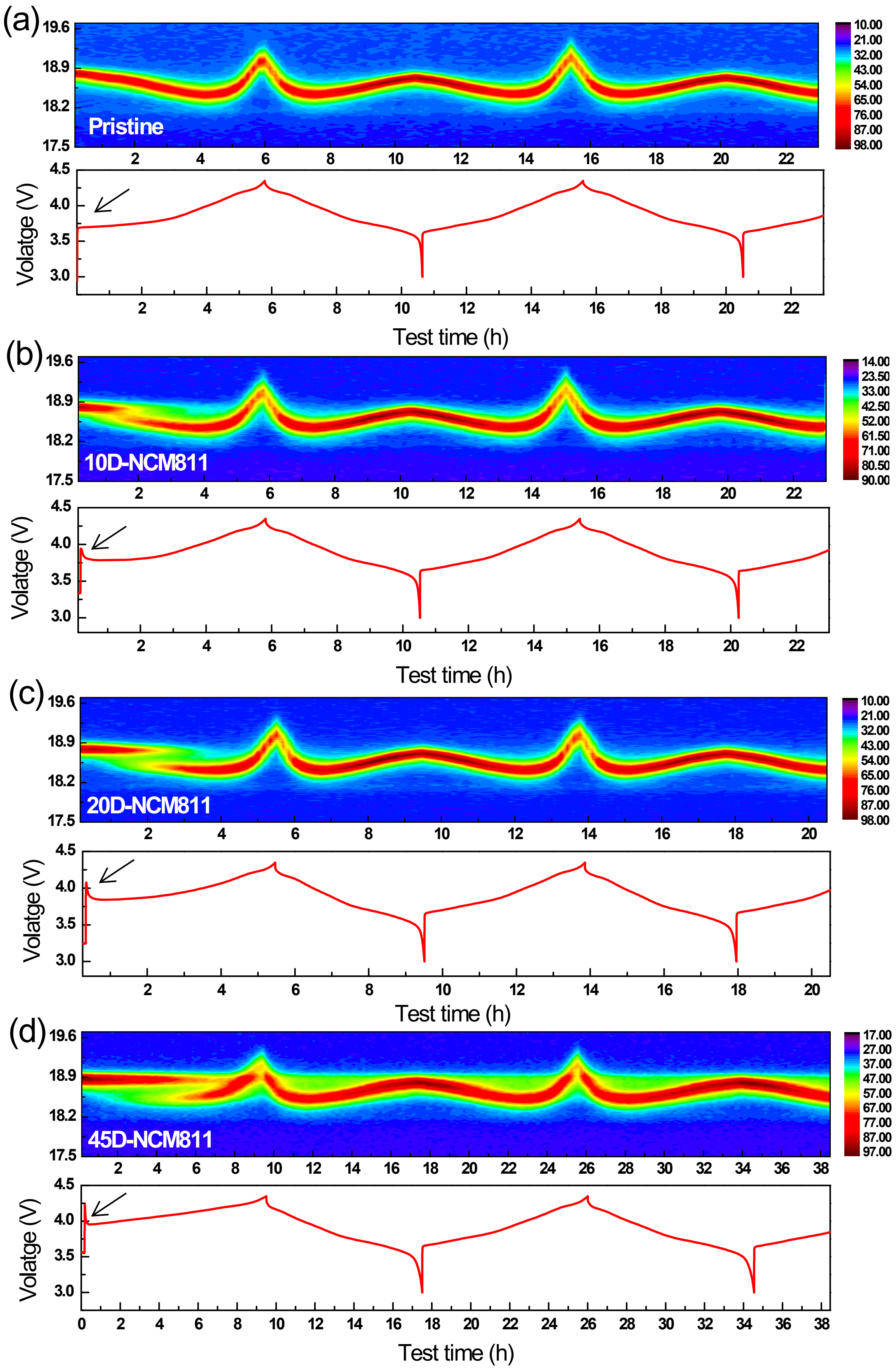

Figure S6 The *in-situ* XRD patterns for (003) peak of NCM811 during charge and discharge and their corresponding charge/discharge curve. (a) pristine NCM811. (b) NCM811 after 10 days' storage. (c) NCM811 after 20 days' storage. (d) NCM811 after 45 days' storage. The *in-situ* XRD patterns display that the "break" at the initial charge grows with the storage time. Noted that the voltage will increase to different values when apply current in the initial charge for pristine, 10D, 20D, 45D samples (marked with black arrow), more explanation will give in Figure S8.

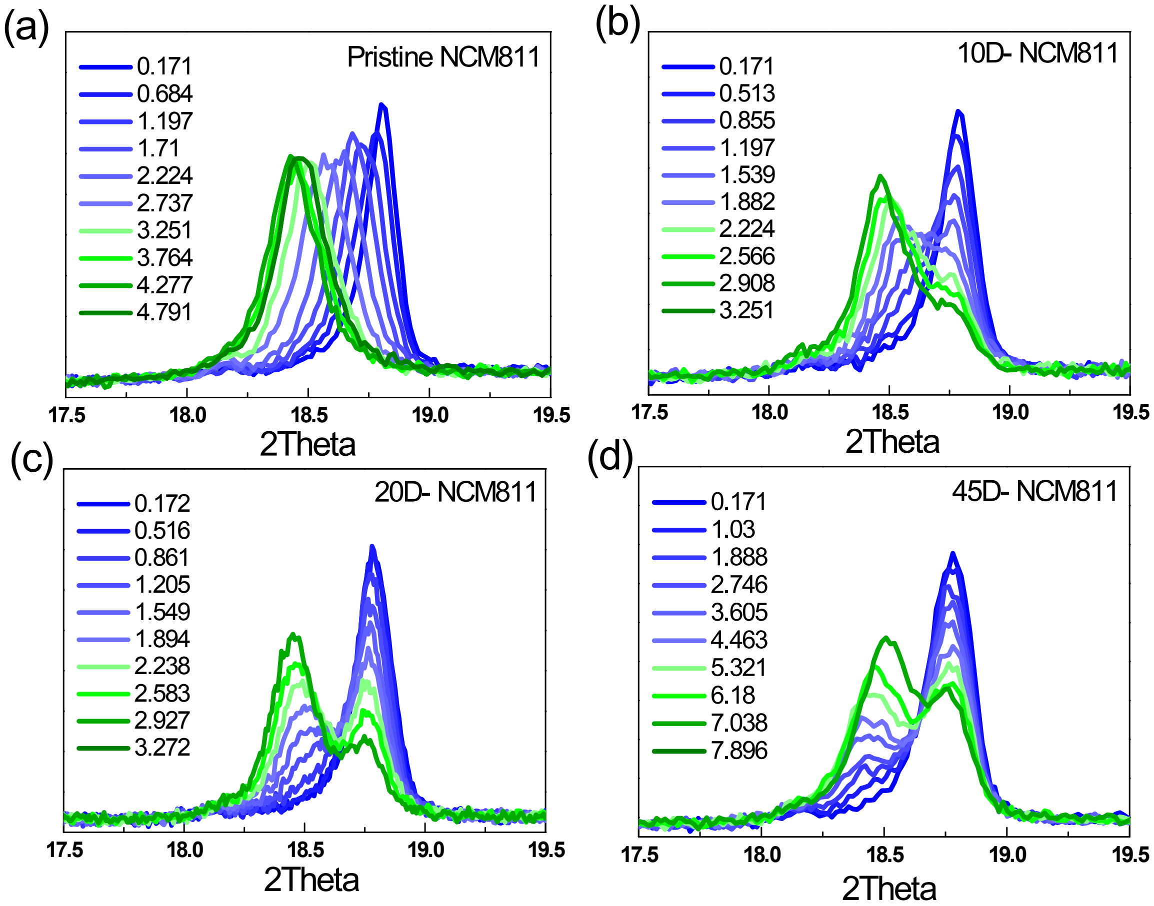

Figure S7 The change of (003) peak with charge time during the initial charge, which is aimed to show the details of "break" area in Figure S6. It can be seen that the (003) peak of pristine NCM 811 stably shift to the small 2θ direction, which means all the particles were transformed with charging. While for the 10D, 20D and 45D samples, the (003) peaks more and more inclined to maintain on their original position, which suggests the growth of Li_2CO_3 film can lead to reaction heterogeneity. In other words, some particles transformed later than others.

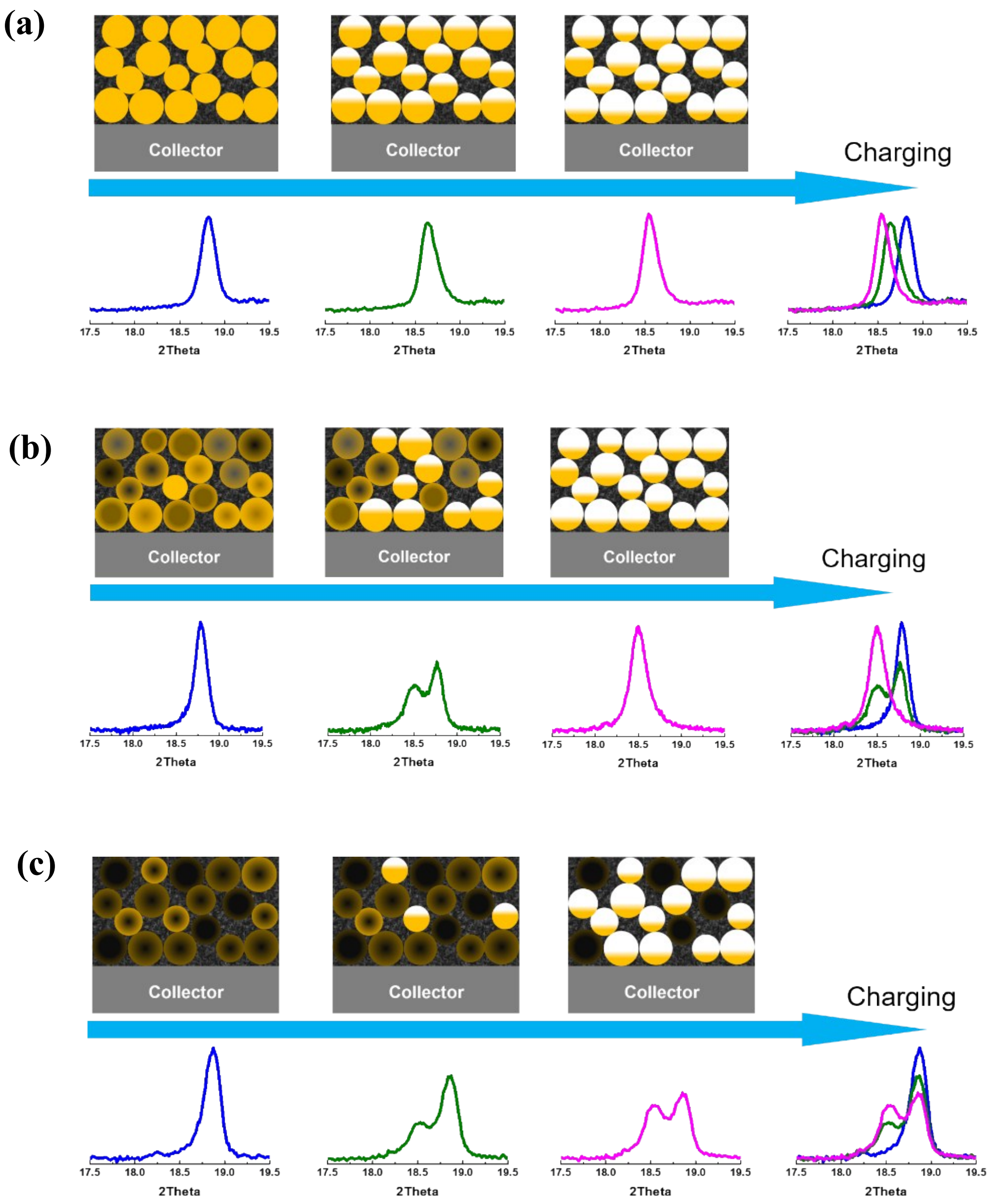

Figure S8. Schematic diagram: The evolution of State-of-Charge heterogeneity and X-ray diffraction patterns for (a) the pristine, (b) the 10D-NCM811 and (c) the 45D-NCM811 samples during charging.

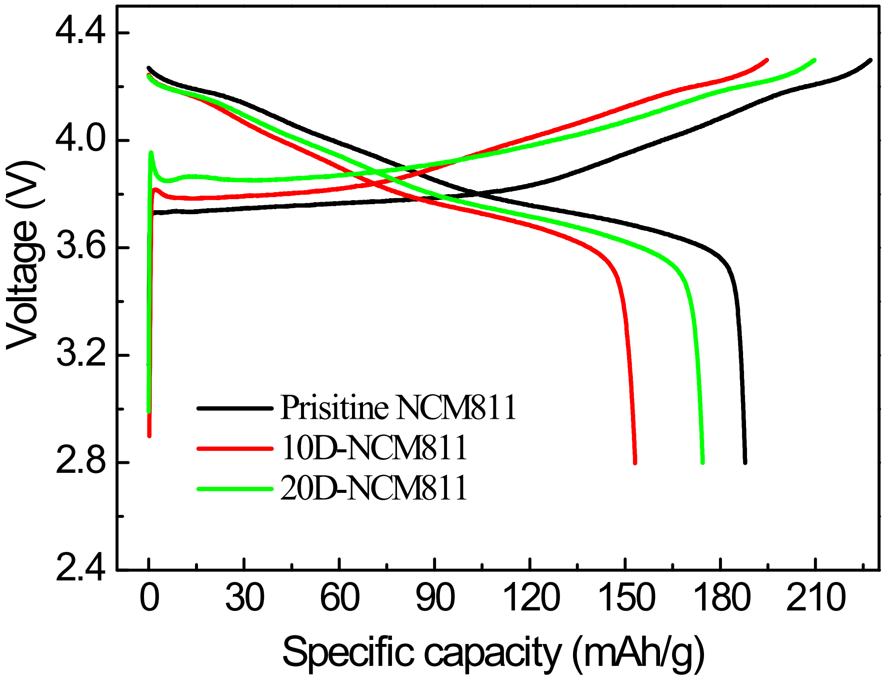

Figure S9. The initial charge-discharge curves of the pristine and stored NCM811.These curves were tested by coin cells at 0.16 C. Obviously, the voltage of 10D-NCM811 increase firstly and then decrease at the beginning of charging, which formed a “swell” in the plot. It is more evident with the increased storage time, as shown in the sample of 20D-NCM811. It is known that the surface of NCM particles is easy to get coated by Li_2CO_3 film during storage, which bring an increased over potential since its poor electronic conductivity. Thus, the energy barrier for lithium extraction increase. When the electrodes were charged, a high energy is needed to overcome the large obstacles and activate the cathodes, which presented as a high potential in the beginning. Once the surface Li_2CO_3 degrades, it will return to normal potential to charge sequentially. When the content of Li_2CO_3 increased, the "swell" would more and more close to the upper cut-off voltage. In this case, the electrode couldn’t be activated. That is the reason that 45D-NCM811 couldn’t charge at 0.16 C. Therefore, the first charge curve could quickly identify the degree of degradation for NCM material by the shape of the "swell". The phenomenon was also observed in Figure S6 in pouch cells.

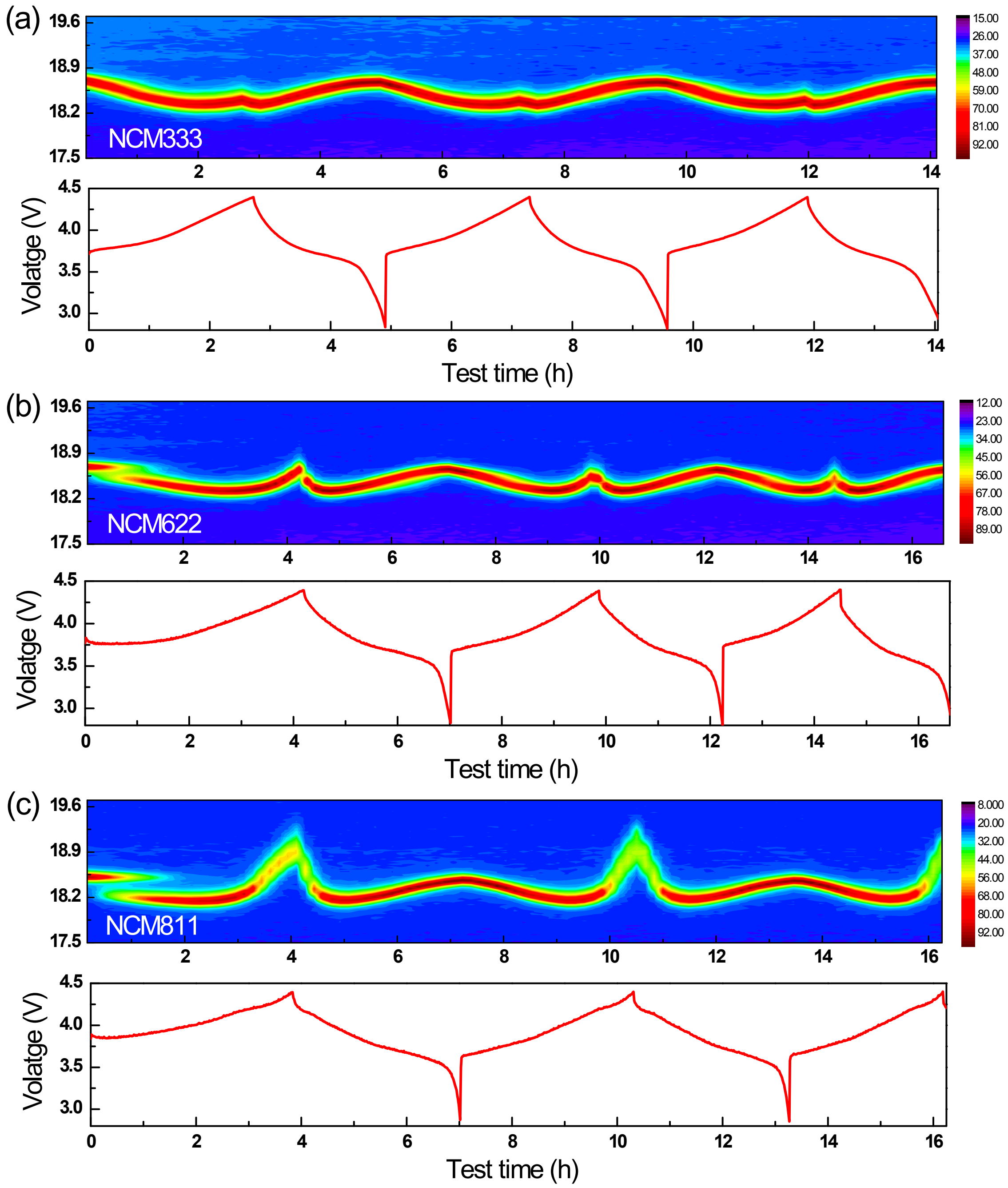

Figure S10 The *in-situ* XRD patterns for (003) peak of NCM cathodes after 20 days' storage during charge and discharge and their corresponding charge/discharge curve. (a) NCM333. (b) NCM622. (c) NCM811.

Figure S11 Three types of aging modes

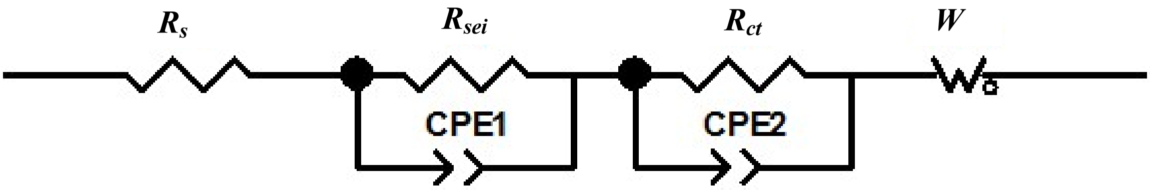

Figure S12 Equivalent circuit model for impedance fitting. The R_s represents the ohmic resistance between the working electrode and the reference electrode. The R_{sei} represents the resistance for Li^+ diffusion in the solid electrolyte interphase layer and R_{ct} represents the charge transfer resistance. The values of R_s, R_{sei} and R_{ct} were listed in Table S4. CPE1 and CPE2 represent constant phase-angel element depicting the non-ideal capacitance of the surface layer and the double layer, respectively. The oblique line in the low-frequency region is assigned to Warburg impedance (W), which is related to the solid state diffusion of Li^+ in the NCM bulk.

Table S1. The ICP-OES results for the chemical composition of the NCM cathodes

Test results	Theoretical value		Experimental value	
Stoichiometric ration	Ni:Co:Mn	Li/(Ni+Co+Mn)	Ni:Co:Mn	Li/(Ni+Co+Mn)
NCM333	0.333:0.333:0.333	1.0	0.328:0.352:0.320	1.057
NCM622	0.60:0.20:0.20	1.0	0.610:0.194:0.196	1.024
NCM701515	0.70:0.15:0.15	1.0	0.709:0.145:0.146	1.002
NCM811	0.8:0.10:0.10	1.0	0.801:0.099:0.100	1.004

The ICP-OES results display that the actual ratios of Ni, Co and Mn in NCMs are consistent with their chemical formula.

Table S2 Rietveld refinement results of XRD patterns for pristine and 45D NCM samples

Samples		a(Å)	b(Å)	c(Å)	V(Å^3)	Cation Mixing	χ^2	R_{wp}	R_p
NCM333	pristine	2.8594(1)	2.8594(1)	14.233(5)	100.7	2.5%	3.34	8.9%	8.2%
	45D	2.8595(2)	2.8595(2)	14.233(5)	100.7	2.5%	3.73	9.4%	8.7%
NCM622	pristine	2.8699(2)	2.8699(2)	14.225(3)	101.4	2.7%	2.00	7.2%	5.8%
	45D	2.8701(2)	2.8701(2)	14.224(3)	101.4	2.7%	2.79	8.7%	6.5%
NCM701515	pristine	2.8710(3)	2.8710(3)	14.212(4)	101.5	1.96%	2.04	6.8%	5.3%
	45D	2.8709(2)	2.8709(2)	14.217(4)	101.5	1.96%	2.37	7.2%	5.6%
NCM811	pristine	2.8725(2)	2.8725(2)	14.203(6)	101.5	1.55%	2.39	6.6%	5.2%
	45D	2.8725(2)	2.8725(2)	14.210(6)	101.5	1.55%	3.10	7.6%	5.8%

The refined cell parameter shows that the *a* axis increases with Ni increase, while the *c* axis decreases with Ni increase. It means the TM-O layers are more compact in the Ni-rich NCM materials. Before and after storage, the cell parameters of NCMs did not change evidently, which indicated the degradation mainly occur at the particle surface.

Table S3. The cycling and rate performance of the pristine and the stored NCM cathodes

Samples	Cycling performance				Rate performance		
	ICE (%)	1st (mAh g^{-1})	100th (mAh g^{-1})	100th/1st (%)	0.2 C (mAh g^{-1})	10 C (mAh g^{-1})	10 C/1 C (%)
Pristine NCM622	87.0	158.9	146.9	92.4	176.5	118.1	66.9
10D-NCM622	86.8	158.7	128.0	80.6	174.0	98.7	56.7
45D-NCM622	31.7	102.7	44.2	43.0	140.3	12.3	8.8
Pristine NCM701515	86.4	171.5	163.6	95.4	186.8	115.2	61.7
10D-NCM701515	87.2	168.2	145.6	86.6	185.7	101.1	54.4
45D-NCM701515	30.1	89	29.6	33.3	Unable to obtain data		
Pristine NCM811	82.6	178.1	176.9	99.3	198.6	122.3	61.6
10D-NCM811	78.7	145.9	152.4	104.5	176.6	92.1	52.2
45D-NCM811	Unable to obtain data						

Table S4. The impedance fitting results of the pristine and the stored NCM cathodes

Samples	Storage time	R_s (Ω)	R_{sei} (Ω)	R_{ct} (Ω)
NCM333	Pristine	0.8	34.8	73
	10 days	1.9	37.6	74.8
	45 days	1.9	39	77
NCM622	Pristine	1.7	42.2	59.3
	10 days	2.2	46.3	73.9
	45 days	2.5	84.0	816.3
NCM701515	Pristine	2.2	39.7	52.7
	10 days	2.5	39.9	57.4
	45 days	2.1	54.3	1402.3
NCM811	Pristine	3.3	42.5	59.6
	10 days	2.6	47.6	90.1
	45 days	2.4	121.6	2238.0

Reference

1. Blum, V.; Gehrke, R.; Hanke, F.; Havu, P.; Havu, V.; Ren, X.; Reuter, K.; Scheffler, M., Ab initio molecular simulations with

numeric atom-centered orbitals. *Computer Physics Communications* **2009,** *180* (11), 2175-2196.

2. Perdew, J. P.; Burke, K.; Ernzerhof, M., Generalized Gradient Approximation Made Simple. *Physical Review Letters* **1996,** *77* (18), 3865-3868.

3. Anisimov, V. V., *Strong coulomb correlations in electronic structure calculations : beyond the local density approximation*. Gordon and Breach: 2000; p 907-931.

4. Monkhorst, H. J.; Pack, J. D., Special points for Brillouin-zone integrations. *Physical review B* **1976,** *13* (12), 5188.

5. Tkatchenko, A.; Scheffler, M., Accurate Molecular Van Der Waals Interactions from Ground-State Electron Density and Free-Atom Reference Data. *Physical Review Letters* **2009,** *102* (7), 073005.

6. Kondrakov, A. O.; Schmidt, A.; Xu, J.; Geßwein, H.; Mönig, R.; Hartmann, P.; Sommer, H.; Brezesinski, T.; Janek, J., Anisotropic Lattice Strain and Mechanical Degradation of High- and Low-Nickel NCM Cathode Materials for Li-Ion Batteries. *The Journal of Physical Chemistry C* **2017,** *121* (6), 3286-3294.

7. K.M., S.; Rao, G. V. S., Performance of layered Li(Ni1/3Co1/3Mn1/3)O2 as cathode for Li-ion batteries. *Electrochimica Acta* **2002**.